Overview of neutron interferometry at NIST

Michael G. Huber[1,a], *Shannon F.* Hoogerheide[1], *Muhammad* Arif[1], *Robert W.* Haun[2], *Fred E.* Wietfeldt[2], *Timothy C.* Black[3], *Chandra B.* Shahi[4], *Benjamin* Heacock[5,6], *Albert R.* Young[5,6], *Ivar A.J.* Taminiau[7], *Dusan* Sarenac[8,9], *David G.* Cory[8,9,10,11], and *Dmitry A.* Pushin[8,9]

[1] National Institute of Standards and Technology, Gaithersburg, MD 20899, USA
[2] Tulane University, New Orleans, LA 70188, USA
[3] University of North Carolina Wilmington, Wilmington, NC 28403, USA
[4] University of Maryland, College Park, MD 20742, USA
[5] North Carolina State University, Raleigh, NC 27695, USA
[6] Triangle Universities Nuclear Laboratory, Durham, NC 27708, USA
[7] Neutron Optics LP, Waterloo, ON N2L0A7, Canada
[8] University of Waterloo, Waterloo, ON N2L3G1, Canada
[9] Institute for Quantum Computing, University of Waterloo, Waterloo, ON N2L3G1, Canada
[10] Perimeter Institute for Theoretical Physics, Waterloo, ON N2L2Y5, Canada
[11] Canadian Institute for Advanced Research, Toronto, ON M5G1Z8, Canada

Abstract. Neutron interferometry at the National Institute of Standards and Technology is a well-established program that performs experiments in a wide range of areas including materials science, quantum information, precision measurements of coherent and incoherent scattering lengths, and dark energy/fifth force searches. Central to the continued success of this program is the further understanding and elimination of instabilities and coherence-losses whether they are from thermal, vibrational, or dynamical sources. We have spent considerable effort in fabricating new interferometer crystals which have higher maximum fringe visibilities and that can be tailored to specific experiments. We describe the current facilities and a new post-machining fabrication process of crystal annealing.

1. Introduction

Interferometry represents one of the most precise instruments for probing fundamental physics using neutrons. This success is despite the fact that neutron interferometry is mostly insensitive to the weak interaction, which is a major focus of fundamental physics and Beyond the Standard Model searches. Neutron interactions with nuclear, magnetic, and gravitational potentials combined with its quantum nature makes neutron interferometry a unique tool for exploring fundamental physics. However, the limited availability of high-quality neutron interferometers has prevented the technique from wider use in the neutron community. One challenge is the physical means by which to produce these types of interferometers. Another challenge is the resulting low flux because the neutron interferometer acts as a very selective momentum filter; the vast majority of neutrons pass through the device without Bragg diffracting. As such, the neutron fluence measured by the detectors is low; on the order of a few neutrons per second. The intensity limitations of neutron interferometry are being addressed [1–3] using a new technique to achieve a Mach-Zehnder interferometer with broad-spectrum acceptance. One issue with this new interferometric technique is that it is devoid of macroscopic spatial separation between the interferometer paths. However, its advantages may prove invaluable for several experiments including precision measurements of gravity.

Perfect-crystal silicon interferometers remain the workhorse of the field. In this proceeding, we discuss recent advances in the fabrication and post-fabrication of silicon interferometers. In addition, we will mention the improvements to stability and noise suppression at the two neutron interferometer facilities at NIST.

1.1. Neutron Interferometry

A perfect-crystal neutron interferometer consists of a silicon ingot machined so that there are several parallel crystal blades on a common monolithic base. A schematic of an interferometer is shown in Fig. 1. Neutrons entering the interferometer Bragg diffract (Laue geometry) in the first (splitter) blade. This coherently separates the neutron into two spatially separate paths labeled I and II. Both neutron paths are Bragg diffracted in a second (mirror) blade and interfere in the final (analyzer/mixer) blade of the interferometer. Conceptually, this is analogous to a Mach-Zehnder interferometer in optics. The two beams exiting the interferometer are historically labeled the O- and H-beams. Neutrons are detected with high efficiency using cylindrical ^{3}He-filled proportional counters. Differences between path I and II modulate the intensity of the O- and H-beams. Typically, a sample called a phase flag is inserted to modulate the signal in a controllable way.

[a] e-mail: michael.huber@nist.gov

© The Authors, published by EDP Sciences. This is an Open Access article distributed under the terms of the Creative Commons Attribution License 4.0 (http://creativecommons.org/licenses/by/4.0/).

Table 1. List of interferometers. Blade width B_w, height B_h and separation $B_{s1,s2}$ are shown. The maximum $\mathcal{V}$ is the largest value that has been observed for any wavelength. Interferometers with contrasts unspecified have either not been used in the last 15 years at NIST and/or are believed to be $< 10\%$. Updated from Ref. [4].

	Name	Type	Lattice Vector	λ Range (nm)	$\mathcal{V}_{\max.}$ (%)	B_w (mm)	B_h (mm)	B_{s1} (mm)	B_{s2} (mm)
1	Poseidon	Skew	(111)	0.33–049	35	2.5	30.0	20.0	36.6
2	Gyges	Skew	(111)	0.22–030	34	1.5	40.0	14.1	82.0
3	Achilles	Skew	(220)	1.00–030	–	2.0	30.0	32.0	25.4
4	Hera	LLL	(111)	0.00–050	90	2.0	25.0	41.5	–
5	Zeus	LLL	(111)	0.00–050	90	2.5	30.4	39.6	–
6	Cronus	LLL	(220)	0.00–020	–	2.5	15.5	34.5	–
7	Hades	Skew	(220)	0.22–025	85	2.8	25.4	16.0	30.5
8	Dionysus	DFS	(220)	0.00–033	25	1.0	16.0	10.0	20.0
9	Aphrodite	LLL	(111)	0.00–054	92	1.0	15.0	10.0	–
10	Iris	2Blade	(111)	0.00–030	80	12.0	30.0	51.0	–

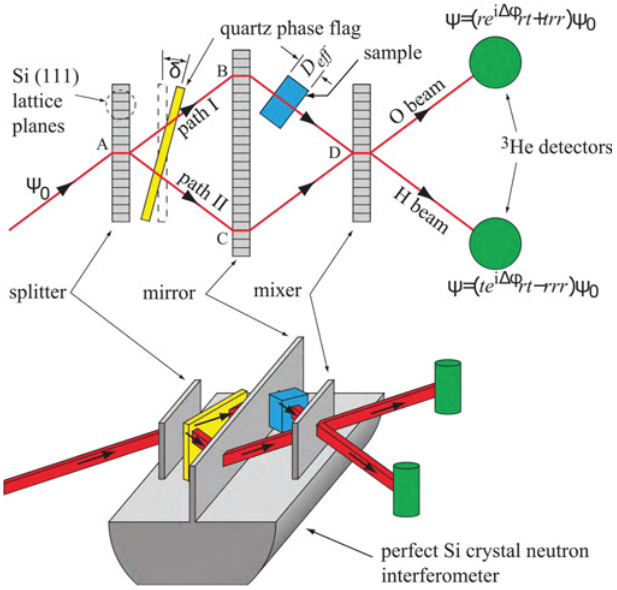

Figure 1. A schematic of a neutron interferometer. Neutrons incident on a crystal blade are Bragg diffracted into two spatially separated paths. These paths interfere with each other in the third or final blade of the interferometer and are detected using two ^{3}He detectors. Differences along the paths modulate the relative intensities of the two detectors.

The effect of neutrons passing through a material is described by an index of refraction n, conceptually the same as for light optics, given by

$$n = \sqrt{1 - \frac{\lambda^2 Nb}{\pi}} \approx 1 - \mathcal{O}(10^{-6}), \tag{1}$$

where λ is the neutron wavelength and Nb is the scattering length density of the material. This gives rise to a phase shift due to an object with thickness D placed inside the interferometer of

$$\phi = (1 - n)kD = -\lambda NbD. \tag{2}$$

Here $k = 2\pi/\lambda$ is the neutron wave vector. The two detectors behind the interferometer measure a signal given by

$$I_O = c_0 + c_1 * \cos[\phi_{\text{flag}}(\delta) + \phi + \phi_0(t)] \tag{3}$$

$$I_H = c_2 - c_1 * \cos[\phi_{\text{flag}}(\delta) + \phi + \phi_0(t)]. \tag{4}$$

The coefficients c_0, c_1, and c_2 are treated as fit parameters. The ratio $\mathcal{V} = c_1/c_0$ is the contrast, or fringe visibility, and is the primary indicator of the quality of an interferometer (absent environmental and experimental factors). More recently, we have begun using another method (discussed in Sect. 3.1) to quantify an interferometer's performance. In this method, the variation in the relative blade thicknesses and angular Bragg plane misalignments between the blades can be measured using refractive elements placed inside the interferometer. This can be done to the precision of a few percent of pendellösung length for relative blade thickness and at the nanoradian level for Bragg plane misalignments. The phase flag provides a phase shift of $\phi_{\text{flag}}(\delta)$ where the angle δ, defined in Fig. 1, changes the flag's effective thickness traversed by the beam paths. The phase $\phi_0(t)$ is phase difference between the two paths of an empty interferometer and drifts with time t as the interferometer is not completely isolated from the environment.

2. NIST facilities

In 2011, the neutron interferometer facility at NIST was expanded to include a secondary beamline. This beamline operates at a fixed $\lambda = 4.4$ Å wavelength, but with a substantial fraction, 23%, of $\lambda/2 = 2.2$ Å such that it can utilize either wavelength for experiments. The facilities' overall characteristics are summarized in Shahi et al. [4,5]. At the time of Ref. [4], the facilities at NIST had 9 interferometer crystals (see Table 1) of varying quality. Since then the interferometer 'Cronus' has been on display at Purdue University and is not available for general use. A new 2-blade interferometer 'Iris' has been machined at Riken and then post-fabricated at NIST. But most notably, the interferometer "Hera", which had low but measurable contrast, has now been greatly improved through annealing [6] and is discussed below.

The secondary neutron interferometry beamline has had a number of experiments including measuring

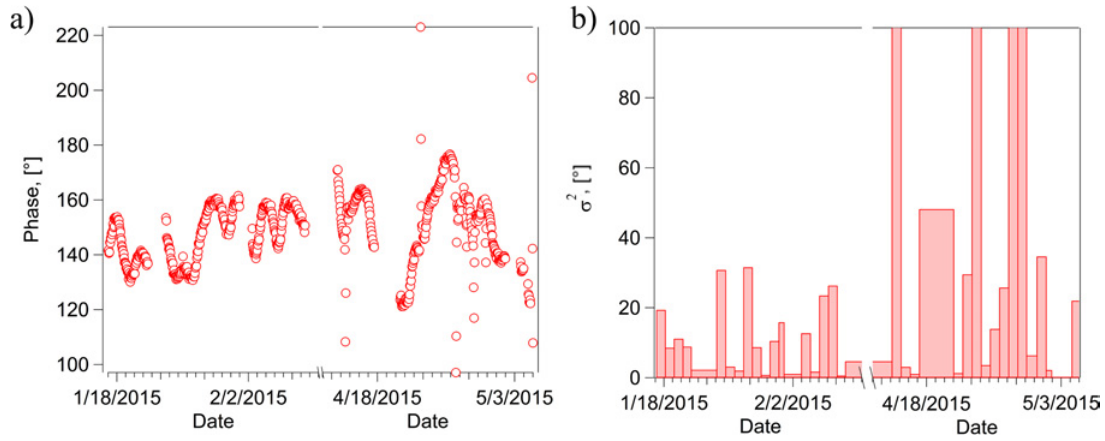

Figure 2. Phase data from a gaseous sample. (a) Phase data taken over a period of several months. Each point represents the fitted ϕ from Eq. (5) taken every 21 minutes. (b) The variance defined in Eq. (5) for the data in (a).

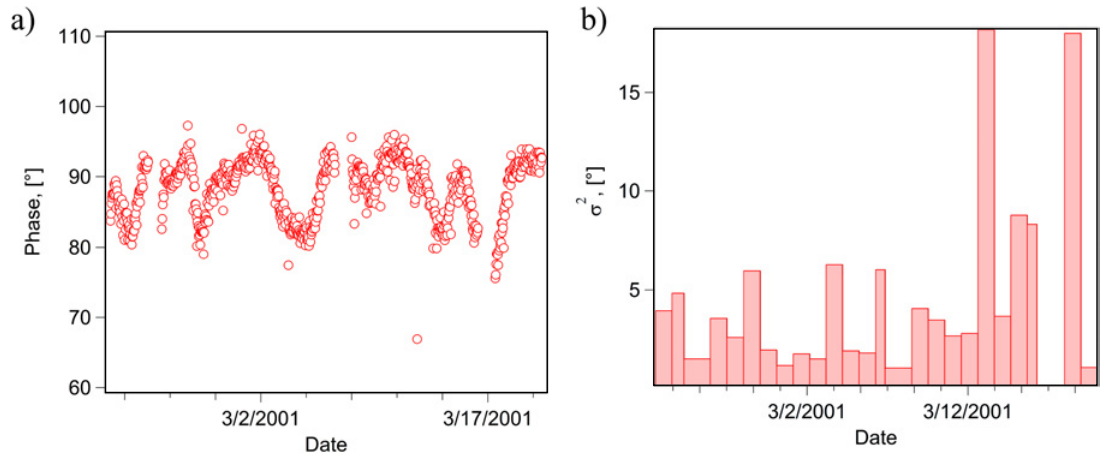

Figure 3. Phase data taken during the deuterium scattering length measurement. (a) Phase data taken over a period of several months. Each point represents the fitted ϕ from Eq. (5) taken every 21 minutes. (b) The variance defined in Eq. (5) for the data in (a).

improved phase stability of an interferometer inside a vacuum chamber [7], characterizing the diffraction pattern of high-aspect-ratio phase gratings [1,2] and sub-micron resolution tomography [8]. Current efforts are to measure pendellösung oscillations in perfect crystals.

The primary interferometry beamline that includes the vibrationally isolated Hutch structure, has been continuing its work on precision scattering length measurements, testing of fabrication techniques and various other items. The capabilities inside the Hutch have not significantly changed since 2011. However, one notable improvement has been in the stability of the interferometer Hutch facility. It was discovered during precision scattering length measurements of helium samples that the phase stability inside the Hutch had degraded over time. The Hutch was designed so that minimum personnel intervention would be required under normal operation. Sample movement, interferometer control, and counting are controlled outside of the facility. To this end, there was a multitude of cables entering the Hutch from small notches along the Hutch floor. Because of the difficulty of subtracting cabling from the Hutch, the majority of these cables were from legacy experiments and not typically utilized. These cables represented a weak but important coupling between the outside NCNR building and the interferometer. To quantify stability we used a variance defined as

$$\sigma^2 = \sum_{i}^{24\ hrs} (\phi_i - \phi_{avg})^2 / N \tag{5}$$

where ϕ_i is the phase of the i^{th} interferogram, ϕ_{avg} is the average measured phase over a 24 hour period and N is the total number of interferograms. A standard interferogram is formed using 21 different phase flag positions stretching over 1.5 periods. For the data shown in Figs. 2–4, neutrons were counted for 60 seconds at each of the 21 phase flag angles. Statistically, this method determines each ϕ_i to an uncertainty of ± 1 degree. In Fig. 2 one can see the phase drifting and large variance of Eq. (5). This is in comparison with data taken measuring the scattering length of deuterium [9] in the earlier days of the facility and is shown in Fig. 3. Removal of these nonessential cabling/connections lead to a 10x increase in stability at the instrument which is now in line with recorded data in 2001 (see Fig. 4). One can see that the original performance has been achieved.

3. Fabrication and annealing

Neutron interferometers are machined from float-zone grown, dislocation-free silicon crystals. In principle

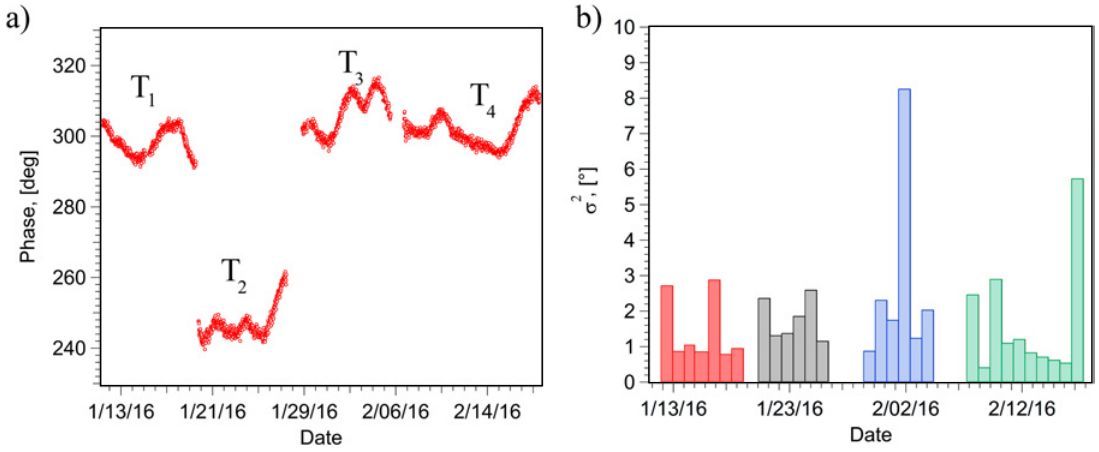

Figure 4. Current phase stability. a) Phase data taken over a period of several months. Each point represents the fitted ϕ from Eq. (5) taken every 21 minutes. b) The variance defined in Eq. (5) for the data in a). The temperature of the interferometer is controlled using a PID feedback loop. The four sections of phase/variance are for different control temperature setpoints.

germanium could also be used for interferometry and is easier to machine than silicon. However, the quality of germanium is not typically sufficient for use in neutron interferometry. The process of fabricating an interferometer is as follows: (1) start with a float-zone perfect silicon crystal ingot; (2) machine the ingot to desired geometry; (3) chemically etching the crystal surfaces; (4) testing the interferometer in a neutron beam; (5) repeating steps (3) and (4) until an acceptable $\mathcal{V}$ is measured. Typically, fabrication is done using a diamond-embedded wheel to cut away material, leaving two or more crystal blades protruding from a common base [10]. This is done with a machining tolerance between (5–7) microns which is roughly 1/10 of the crystal's pendellösung length. The base not only adds stability but ensures that the lattice planes of each blade are aligned relative to each other. Diamond wheels and other cutting techniques leave subsurface damage and micro cracking in the surface layers that may extend up to 100 microns into the crystal blade. This damaged layer completely destroys the contrast of the interferometer. Therefore, the interferometer surfaces are chemically etched to remove any layers of machining damage. After etching the interferometer's contrast is measured using a neutron beam. The etching and testing of the interferometer is typically done iteratively until reasonable contrast is obtained [11, p. 32–34]. Etch rates vary along the length of the crystal blades with the etchant more efficiently removing silicon at the ends of crystal. The nonuniform etching rates lens the blade's surface causing thickness variations on the order of microns [10] which in turn destroys contrast and is why an iterative etching process is done. It is not guaranteed that contrast can be measured in a new interferometer as the bulk features of the crystal and other factors may still dominate.

3.1. Qualitative stress analysis

One often thinks of Bragg diffraction as a simple geometric effect and that for a neutron incident on a crystal lattice, an incident beam will be diffracted at a precise angle θ_{Bragg}. In fact, Bragg diffraction occurs over a small angular range of $\theta_{\text{Bragg}} \pm \Delta_{\text{D}}$ where Δ_{D} is the Darwin width and is typically only a few arcseconds wide. For a crystal with structure factor $|F_H|$

$$\Delta_{\text{D}} = \frac{\lambda^2 |F_H|}{\pi a^3 \sin(2\theta_{\text{Bragg}})} \tag{6}$$

where a^3 is the volume of a unit cell. Because this angle is only a few arcsconds, neutron interferometers are machined out of single ingots and preserve a large common base in addition to the diffracting crystal blades. This ensures that the lattices of each diffracting blade observe the original ingot's uniformity and are aligned to within the Darwin width of each other. If this was not the case, neutron interference would not be observed after the final blade of the interferometer. Stresses internal to the interferometer can cause these diffracting planes to be slightly misaligned. Neutron diffraction inside a crystal lattice is highly sensitive to misalignments in the incident angle θ which can be modified using optical elements. For instance, because the index of refraction for neutrons is so close to unity, very small deflections can be achieved though fused silica prisms. Here we used a right angle circular prism [12] inserted inside the interferometer to deflect the incident neutron while maintaining the Bragg condition and allowing the study of diffraction effects and stresses in the crystal. The prism had a pitch angle of $\alpha = 6^\circ$, which gives a total beam deflection of, to first order,

$$\delta(\varphi) = \frac{\lambda^2}{2\pi} Nb \tan(\alpha) \sin(\varphi) \tag{7}$$

where φ is the angle between the Bragg plane and the prism deflecting plane.

Placing the prism in path II of the interferometer (see Fig. 5) and blocking path I allows the measurement of multiple Bragg reflections with resulting intensities

$$I_{\text{RR}} \propto \mathcal{I}[\delta(\varphi) + \delta^{\text{rel}}_{\text{S,M}}, \Delta_{\text{M,S}}] \tag{8}$$

$$\begin{aligned} I_{\text{RRR}} \propto\ & \mathcal{J}[\delta(\varphi) + \delta^{\text{rel}}_{\text{S,M}}, \Delta^{\text{rel}}_{\text{M,S}}] \\ & + \mathcal{J}[\delta^{\text{rel}}_{\text{S,M}} - \delta^{\text{rel}}_{\text{S,A}}, \Delta_{\text{A,S}} - \Delta_{\text{M,S}}] \\ & + \mathcal{J}[\delta(\varphi) + \delta^{\text{rel}}_{\text{S,A}}, \Delta_{\text{A,S}}] \end{aligned} \tag{9}$$

are both functions of the relative angle δ^{rel} between the diffracting planes and relative blade thickness

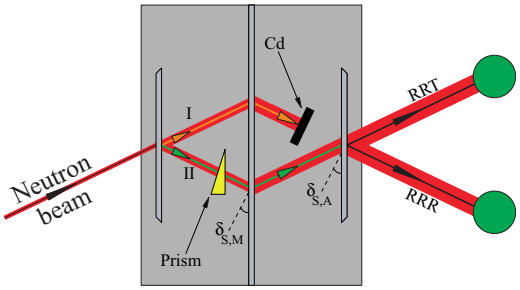

Figure 5. Setup to measure the RR and RRR intensities (Eqs. (8) & (9)) as function of prism angle. Cadmium, 1 mm thick, is used to completely absorb path I. The RR intensity is a summation of the outgoing RRT and RRR beams.

Figure 6. The large tube Furnace [14] used in the annealing work of Ref. [6].

difference Δ. The subscript 'S' refers to the splitter or first blade of the interferometer, 'M' the mirror blade, and 'A' the analyzer or final blade. Both functions $\mathcal{I}$ and $\mathcal{J}$ are ideally written in terms of Bessel functions but allow for non-ideal behavior [13]. Details can be found Ref. [6].

The measured relative misalignments of 'Hera' were large enough to explain its historically low contrast. In order to realign the crystal blades at the 10 nrad level 'Hera' was annealed in a 208 mm ID tube furnace which is shown in Fig. 6. As seen in Fig. 7, the interferometer rested on a silicon wafer supported by ceramic crucible. Argon gas flowed continuously through the furnace. The temperature was ramped at a rate of 5 °C/min and held for 10 hours at 800 °C. The interferometer was then cooled down over a period of 17 hours.

We found that the Bragg plane misalignment gradient dropped from 10 nrad/mm to less than 5 nrad/mm after annealing, and the absolute misalignment between the mirror and analyzer blades also decreased for some

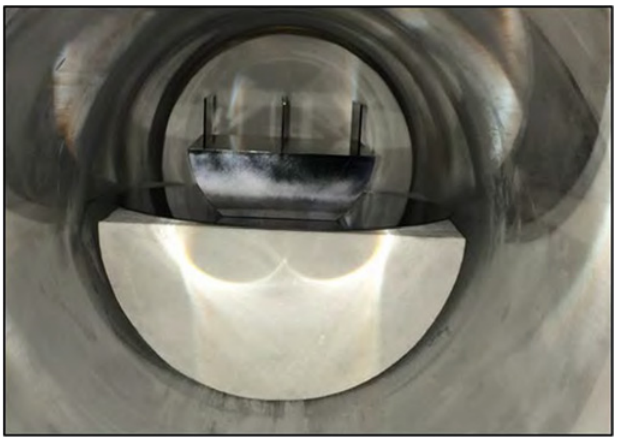

Figure 7. 'Hera' inside the tube furnace.

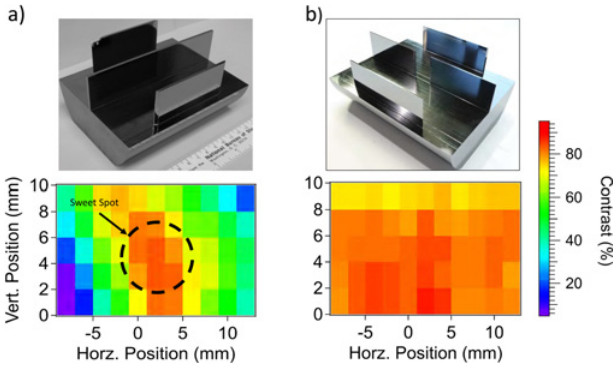

Figure 8. A comparison of "Zeus" which has been the most prolific neutron interferometer at NIST with "Hera" post heat treatment. One can see that the contrast of "Hera" is now both high and uniform across its front surface. The crystal "Zeus" exhibits typical behavior where contrast is highest only for a limited area or sweet spot.

portions of the interferometer. Most importantly, we found an increase in contrast from 23% to 90% [6].

The crystals "Zeus" and "Hera" are nearly physically identical (photos of which are shown in Fig. 8) and were machined at the same facility around similar times; thus we expect structurally very little difference between the two interferometers. However, prior to heat treatment "Hera" only obtained a maximum contrast of 23%. As reported in Heacock et al. [6], to verify the prism measurements, we measured the contrast of "Hera" both before and after annealing. Figure 8 shows uniform contrast measured across the crystal surface of "Hera" post heat-treatment. For comparison, "Zeus", the most widely used interferometer at NIST because of its repeatability high 85% contrast, is also shown. Note that in practice, most interferometers have a narrow range called the sweet spot where one obtains the maximum contrast and outside of this sweet spot the contrast is significantly worse. One can see this spot in Fig. 8a for "Zeus". In addition to "Hera", the baby interferometer, "Aphrodite", has also been recently re-machined and annealed. The resulting contrast was 92% compared to <30% before.

4. Conclusion

We have successfully demonstrated that annealing interferometer crystals has a positive effect on the

interferometer's performance and is the first non-chemical method to do so. By relieving internal crystal stresses through heat treatment, we hope that this less-destructive method leads to higher-contrast interferometers with more uniform phase deviations. In addition, using prism deflection we can measure and quantify imperfections of the interferometer in a way that is more sensitive than comparing the overall contrast of the device. Our aim is that post-fabrication, improved environmental isolation, and utilization of lessons from quantum information will make neutron interferometry a more robust measurement technique and increase its usefulnesses in other applications.

This work is part of several on-going collaborations whose individual contributions are numerous. Special thanks goes to Professors M. W. Snow, K. Hirota, M. Kitaguchi, H. Shimizu; NIST staff C. W. Clark, W. Chen; RIKEN's Y. Yamagata, Sugawara, T. Hosobata, M. Takeda; Waterloo Postdoc T. Mineeva; students K. Li, J. Nsofini, P. Saggu, A. Kowler, T. Yamamoto, A. Okada; finally, E. Baltic and the NCNR for their technical assistance.

This work was supported in part by the US Department of Energy under Grant No. DE-FG02-97ER41042, National Science Foundation Grant Nos. PHY-1307426 and PHY-1205342, Canadian Excellence Research Chairs (CERC) (No. 215284), the Canada First Research Excellence Fund (CFREF), Natural Sciences and Engineering Research Council of Canada (NSERC) Discovery (No. RGPIN-418579), Collaborative Research and Training Experience (CREATE) (No.414061), and the NIST Quantum Information Program.

References

[1] P.A. Pushin, *Three Phase-Grating Moire Interferometer* (2018), International Workshop on Particle Physics at Neutron Sources

[2] D. Sarenac, D.A. Pushin, M.G. Huber, D.S. Hussey, H. Miao, M. Arif, D.G. Cory, A.D. Cronin, B. Heacock, D.L. Jacobson, et al., Phys. Rev. Lett. **120**, 113201 (2018)

[3] D.A. Pushin, D. Sarenac, D.S. Hussey, H. Miao, M. Arif, D.G. Cory, M.G. Huber, D.L. Jacobson, J.M. LaManna, J.D. Parker et al., Phys. Rev. A **95**, 043637 (2017)

[4] C.B. Shahi, M. Arif, D.G. Cory, T. Mineeva, J. Nsofini, D. Sarenac, C. Williams, M.G. Huber, D.A. Pushin, Nucl. Inst. and Meth. A **813**, 111 (2016)

[5] D.A. Pushin, M.G. Huber, M. Arif, C.B. Shahi, J. Nsofini, C.J. Wood, D. Sarenac, D.G. Cory, Adv. High Energy Phys., 687480 (2014)

[6] B. Heacock, M. Arif, D.G. Cory, T. Gnaeupel-Herold, R. Haun, M.G. Huber, M.E. Jamer, J. Nsofini, D.A. Pushin, D. Sarenac et al., Rev. Sci. Inst. **89**, 023502 (2018)

[7] P. Saggu, T. Mineeva, M. Arif, D.G. Cory, R. Haun, B. Heacock, M.G. Huber, K. Li, J. Nsofini, D. Sarenac et al., Rev. Sci. Inst. **87**, 123507 (2016)

[8] B. Heacock, D. Sarenac, D.G. Cory, M.G. Huber, J. Maclean, H. Mao, H. Wen, D. Pushin (2018), 1808.07476

[9] K. Schoen, D.L. Jacobson, M. Arif, P.R. Huffman, T.C. Black, W.M. Snow, S.K. Lamoreaux, H. Kaiser, S.A. Werner, Phys. Rev. C **67**, 044005 (2003)

[10] M. Zawisky, J. Springer, R. Farthofer, U. Kuetgens, Nucl. Inst. Meth. A **612**, 338 (2010)

[11] H. Rauch, S.A. Werner, *Neutron Interferometry: Lessons in Experimental Quantum Mechanics, Wave-Particle Duality, and Entanglement*, 2nd edn. (Oxford University Press, 2015)

[12] D.A. Pushin, D.G. Cory, M. Arif, D.L. Jacobson, M.G. Huber, Appl. Phys. Lett. **90**, 224104 (2007)

[13] D. Petrascheck, H. Rauch, Acta Crystallogr. A **40**, 445 (1984)

[14] Certain trade names and company products are mentioned in the text or identified in an illustration in order to adequately specify the experimental procedure and equipment used. In no case does such identification imply recommendation or endorsement by the National Institute of Standards and Technology, nor does it imply that the products are necessarily the best available for the purpose